Analysis of Plasma Impedance in Helicon Antenna Thrusters

IEPC-2015-326/ISTS-2015-b-326

Presented at Joint Conference of 30th International Symposium on Space Technology and Science, 34th International Electric Propulsion Conference and 6th Nano-satellite Symposium
Hyogo-Kobe, Japan
July 4–10, 2015

Bin Tian* and E. Ahedo†
Universidad Carlos III de Madrid, Madrid, 28911, Spain

J. Navarro-Cavalle ‡
Universidad Politecnica de Madrid, Madrid, 28040, Spain

Abstract: The parametric investigation of plasma-wave interaction in an Helicon Antenna Thruster is carried out. The plasma impedance of two mainly used antenna families are compared to choose the optimum antenna and geometry parameters. And, the characteristics of plasma-wave interaction near the lower hybrid frequency are analyzed. The full wave propagation regimes and the effect of parameter variations on the plasma resistance are discussed.

I. Introduction

The Helicon Antenna Thruster (HAT) is a new concept of electric propulsion, which generates thrust by electrodeless acceleration of plasma.[1–3] As the core component of HAT, the helicon source, which can produce high plasma density with relatively low magnetic fields, plays a significant role in thruster performances. The mechanism of plasma formation in helicon sources has been researched extensively in recent decades.[5–7] Efficient wave-plasma energy conversion and fully plasma ionization are the aims of a high-quality helicon source.

In order to optimize the helicon source, the antenna-plasma Impedance is used to measure the efficiency of the antenna-plasma coupling. To this respect, maximizing the antenna resistance is proposed as a main optimization criterion.[8] Therefore, considering the principle and structure of helicon source, two key aspects should be taken into account. The first one is the optimization of antenna design. The shape of antennas influences the performance of the helicon source largely because of the different mode excitation and the ability of coupling energy to the plasma.

Secondly, the investigation of parametric regimes of the wave propagation is very necessary in order to select the antenna frequency and the magnetic strength. In our previous studies,[12] the parametric analysis was carried out when the operating frequency ω was much larger than the lower hybrid frequency ω_{lh}. An estimated scaling law for the optimum performance of helicon source was achieved. However the more conventional operating frequency of helicon plasmas is between the lower hybrid frequency ω_{lh} and the electron cyclotron frequency ω_{ce}. Moreover, several experimental and theoretical studies suggest that an optimal frequency could be close to the lower hybrid frequency.[13,14]

In this framework, 1D radial model of wave-plasma interaction is implemented in section II to study the wave propagation and the antenna optimum performance. Two main antenna families, Double saddle and Helical series are analysed in section III. A parametric investigation near the lower hybrid frequency is illustrated in section IV to look for conditions maximizing the plasma resistance. Section V gives conclusions.

*PhD Student, Plasmas and Space Propulsion Team, UC3M, 88tian33@gmail.com.
†Professor, Plasmas and Space Propulsion Team, UC3M, eduardo.ahedo@uc3m.es.
‡PhD Student, Plasmas and Space Propulsion Team, UPM, jaume.navarro@upm.es.

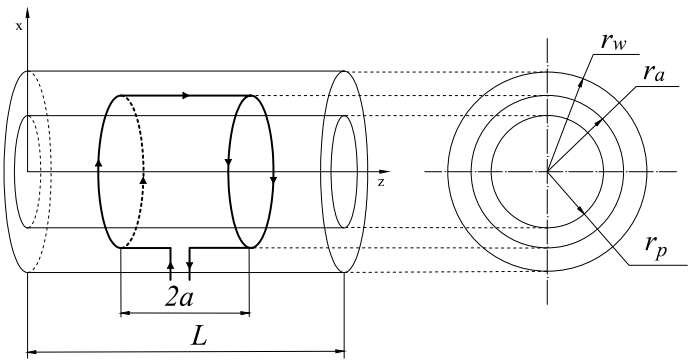

Figure 1. Helicon source model.

II. Theory

A. 1D Plasma-wave simulation Model

The available 1D cylindrical model, with a purely axial magnetic field, is used for the parametric investigation here. We consider a cylindrical source of length L and radius r_p filled with a fully-ionized plasma. The radial variation of the plasma density, $n = n(r)$, is known. The plasma source is surrounded by an antenna, which is assumed infinitely thin and located at $r = r_a$, with $r_a > r_p$. Different shapes of antennas will be analysed; the antenna shown in Fig. 1 is called Nagoya III type. The plasma is confined radially by the applied axial magnetic field B_0, created by a set of external coils (which are assumed to have no effects on the plasma-wave interaction). The whole set is immersed in a larger conducting vessel (i.e. a Faraday cage, the vacuum chamber, etc,.) of length L and radius r_w with $r_w > r_a$.

The antenna emits electromagnetic radiation of frequency ω, of the order 1-30 MHz. We look for the linear interaction of the RF emission with the plasma. The linear plasma-wave response varies as $\exp(-i\omega t)$ and is governed by Maxwell equations:

$$\nabla \times \boldsymbol{E} = i\omega \boldsymbol{B} \tag{1}$$

$$\nabla \times \boldsymbol{B} = \mu_0(-i\omega \overline{\overline{\epsilon}} \cdot \boldsymbol{E} + \boldsymbol{j}_a) \tag{2}$$

where: $\boldsymbol{E}$ and $\boldsymbol{B}$ represent only the RF-related electromagnetic field, $\boldsymbol{j}_a$ is the external current density from the antenna, $\overline{\overline{\epsilon}}$ is the plasma dielectric tensor, Fourier expansion in time has been applied, and all magnitudes are expressed in complex form.

For a cold, weakly-collisional plasma, the dielectric tensor takes the form[15]

$$\overline{\overline{\epsilon}} = \epsilon_0 \begin{bmatrix} \kappa_1 & i\kappa_2 & 0 \\ -i\kappa_2 & \kappa_1 & 0 \\ 0 & 0 & \kappa_3 \end{bmatrix} \tag{3}$$

$$\kappa_1 = 1 - \sum_j \frac{\omega_{pj}^2 (\omega + i\nu_j)}{\omega \left[(\omega + i\nu_j)^2 - \omega_{cj}^2 \right]}, \tag{4}$$

$$\kappa_2 = -\sum_j \frac{s_j \omega_{cj} \omega_{pj}^2}{\omega \left[(\omega + i\nu_j)^2 - \omega_{cj}^2 \right]}, \tag{5}$$

$$\kappa_3 = 1 - \sum_j \frac{\omega_{pj}^2}{\omega (\omega + i\nu_j)} \tag{6}$$

where ω_{cj} and ω_{pj} are the cyclotron and electrostatic frequencies (of species $j = i, e$), ν_j is the collision frequency and s_j is the sign of the electric charge.

For the finite length cylinder source, the plasma is bounded by conducting plates at both ends. Therefore, the reflection boundary conditions: $E_r(0) = E_\theta(0) = E_r(L) = E_\theta(L) = 0$ are achieved at the two conducting end-walls. Then, EM field components can also be expanded in the following (z, θ) Fourier series,[10]

$$\begin{pmatrix} E_r(r,\theta,z,t) \\ E_\theta(r,\theta,z,t) \\ B_z(r,\theta,z,t) \end{pmatrix} = \sum_{l,m} \begin{pmatrix} E_r^{(l,m)}(r) \\ E_\theta^{(l,m)}(r) \\ B_z^{(l,m)}(r) \end{pmatrix} \sin\left(\frac{l\pi}{L}z\right) \exp\left[i\left(m\theta - \omega t\right)\right] \tag{7}$$

$$\begin{pmatrix} B_r(r,\theta,z,t) \\ B_\theta(r,\theta,z,t) \\ E_z(r,\theta,z,t) \end{pmatrix} = \sum_{l,m} \begin{pmatrix} B_r^{(l,m)}(r) \\ B_\theta^{(l,m)}(r) \\ E_z^{(l,m)}(r) \end{pmatrix} \cos\left(\frac{l\pi}{L}z\right) \exp\left[i\left(m\theta - \omega t\right)\right] \tag{8}$$

where $k_l = l\pi/L$ is the parallel wavenumber; m is integer and l is natural.

Considering the geometry of the antenna, the general form of the antenna current density is

$$\boldsymbol{j}_a(\boldsymbol{r},t) = I_a \delta(r - r_a)\left[\mathbf{1}_z s_z(\theta,z) + \mathbf{1}_\theta s_\theta(\theta,z)\right] \exp(-i\omega t) \tag{9}$$

where I_a is the antenna current and s_z and s_θ define the linear shape of the antenna.[22] This antenna current density is expanded as

$$j_\theta(r,\theta,z,t) = \sum_{m,l} j_\theta^{(l,m)}(r) \sin\left(\frac{l\pi}{L}z\right) \exp\left[i\left(m\theta - \omega t\right)\right] \tag{10}$$

$$j_z(r,\theta,z,t) = \sum_{m,l} j_z^{(l,m)}(r) \cos\left(\frac{l\pi}{L}z\right) \exp\left[i\left(m\theta - \omega t\right)\right] \tag{11}$$

The geometry and corresponding Fourier expansion for different type of antennas will be introduced in detail in next section. Then, Maxwell equations can be simplied and solved numerically as an ordinary differential problem in radially uniform and nonuniform plasma density cases.[7] All EM filed components can be obtained. For radially uniform density case, the solutions can be expressed as the combination of Bessel functions. This analytical method has benn introduced by Shamrai[6] and Cho[10] in details.

B. Antenna-plasma impedance

The antenna-plasma impedance can be discussed once the electromagnetic fields are determined. As it is known, the voltage bias U_a at the antenna terminals is calculated as

$$U_a = -\oint_{l_a} \boldsymbol{E} \cdot d\boldsymbol{l} \tag{12}$$

where the integration is along the total antenna path l_a, and the antenna current I_a leads to define the antenna impedance Z as,

$$Z = R - iX = \frac{U_a}{I_a}, \tag{13}$$

where $R = Re(Z)$ is the antenna resistance and $X = Im(Z)$ is the reactance. In principle the reactance would be obtained from the imaginary contribution of the antenna terminals bias voltage

$$X = -\frac{Im(U_a)}{I_a}, \tag{14}$$

However, in the present zero-thickness antenna model, some of the electric field components involved in the computation of the reactance becomes infinite at the antenna location so that the reactance would be infinite. Therefore, the reactance which is limited by the cross-sectional thickness of the antenna cannot be computed with the ideal model. Shamrai mentioned this phenomenon in Ref. [9] and use the "dry" antenna reactance to estimate the plasma reactance. Besides, for a given antenna the reactance seems to be little affected by the operational conditions. Thus, maximizing the antenna resistance is proposed as a main optimization criterion.[23]

In a classical antenna theory, the antenna resistance is constituted of the internal resistance and radiation resistance. In our 1D model the antenna wire is assumed as a perfect conductor so that the internal resistance is zero. Thus, all the power emitted by the antenna is absorbed in the plasma column. Then, the time-averaged resistive, electric power at the antenna terminals is

$$P_{total} = \frac{I_a^2 R}{2}. \tag{15}$$

This total emitted power must be equal to the power absorbed by the plasma column. We compute next this power and the comparison of this two methods will serve as the validation of the model. Hence, the time-averaged power density absorbed by the plasma at a given location (r, θ, z) is

$$p_{abs} = \frac{1}{2}\mathrm{Re}\left(\boldsymbol{E}^* \cdot \boldsymbol{j}\right) = \frac{1}{2}\mathrm{Re}\left(\boldsymbol{E}^* \cdot \overline{\overline{\sigma}} \cdot \boldsymbol{E}\right) \tag{16}$$

where $\overline{\overline{\sigma}} = -i\omega\overline{\overline{\epsilon}}$ is the plasma conductivity tensor . The fields **E** are the sum of all the l,m modes. Next, averaging over z and θ, the radial distribution of power density can be defined as

$$P_{abs}(r) = \int_0^{2\pi}\int_0^{L} p_{abs}(r,\theta,z)d\theta dz = -\frac{1}{2}\pi\omega L \sum_{l,m}\mathrm{Im}\left[E^*_{(l,m)}(r)\cdot\overline{\overline{\epsilon}}^*(r)\cdot E_{(l,m)}(r)\right] \tag{17}$$

The total absorbed power is the integration in the whole plasma volume

$$P_{total} = \int_0^{2\pi}\int_0^{L}\int_0^{r_p} p_{abs}(r,\theta,z)\cdot r dr d\theta dz = \int_0^{r_p} P_{abs}(r)\cdot r dr. \tag{18}$$

It has been checked that, within numerical accuracy, this computation yields the same result with Eq. (15).

C. Nominal Simulation case

With the purpose of optimising the thruster, the parametric investigation of the helicon source is based on a particular design of 15kW HAT.[24] The gas is argon, the radially cold, uniform plasma and axial static magnetic field are taken into account. The main parameters are summarized in Tab. 1. These parameters are used in all the calculations, except for the one whose variation is being studied.

Parameter		**Value**
r_p	Plasma radius	$0.0735m$
L	Plasma and cage axial length	$5r_p$
r_w	External cage radius	$2r_p$
B_0	Applied magnetic field	$450G$
T_e	Plasma temperature	$20eV$
n_0	Plasma density	$5.6\times10^{18}m^{-3}$
ν_e	Electron collision frequency	$3.26MHz$
f_{RF}	Frequency of the RF emission	$13.56MHz$
r_a	Antenna loop radius	$1.05r_p$
$L_a = 2a$	Antenna axial length	$L/2$
z_a	Antenna symmetry plane	$L/2$

Table 1. Summary of input data for the plasma-wave interaction simulations.

III. Optimization of Antenna Design

In this section, comparative studies have been carried out for the double saddle and helical antennas. The Nagoya III antenna is the shape connecting the two families.

(a) Nagoya III antenna (b) Double saddle antenna (c) Half-turn helical antenna (d) 1-turn helical antenna

Figure 2. Different types of antennas.

A. Description of antennas

The current distribution of several types of antennas shown schematically in Fig. 2 is calculated. For all antennas, the radius of the antenna wire is neglected and the antenna is located in the surface $r = r_a$. Therefore, the radial component of current density j_a is zero. We assume that the electrostatic fields are shielded from the plasma so that the antenna current is divergence-free

$$\nabla \cdot \boldsymbol{j}_a = 0 \tag{19}$$

Hence, the relation between the amplitude of azimuthal component and axial component is

$$j_\theta^{(l,m)} = -i\frac{k_l r_a}{m} j_z^{(l,m)} \tag{20}$$

The azimuthal component j_θ can be easily obtained once j_z is determined. Next, based on the different geometry, the expression of current density for each type of antennas is discussed.

1. Nagoya III antenna

The Nagoya III antenna is shown in Fig. 2(a) and is widely used in industrial applications. The two circle loops on either side of the antenna are connected by straight wires. Using the Fourier transform, the current density can be written as

$$j_z^{(l,m)}(r) = \frac{2I_a}{\pi^2 l r_a}\cos\left(\frac{l\pi}{L}z_a\right)\sin\left(\frac{l\pi}{L}a\right)\delta(r - r_a) \tag{21}$$

where δ is the Dirac function, z_a is the position of the center of antenna and a is the half-length of the antenna. Additionally, the azimuthal current j_θ can be easily obtained using Eq. (20).

2. Double saddle family

Fig. 2(b) shows the double saddle antenna, which becomes the Nagoya type III antenna when the azimuthal elements extend to an angle π. The differences between these two antennas are the increase of axial elements and the decrease of azimuthal elements. The expression of the current density is

$$j_z^{(l,m)}(r) = \frac{2I_a}{\pi^2 l r_a}\cos\left(\frac{l\pi}{L}z_a\right)\sin\left(\frac{l\pi}{L}a\right) sin\left(\frac{m\pi}{2}\right) sin\left(\frac{m\theta_t}{2}\right)\delta(r - r_a) \tag{22}$$

where θ_t is the angle of the arc part.

3. Helical family

Fig. 2(c) and Fig. 2(d) show helical antennas with half and one turns cases($n = 0.5$ and $n = 1$). Because of their geometry, wave energy vectors propagate mainly along the magnetic field. According to the helix geometry, the current density j_z is

$$\begin{aligned} j_z^{(l,m)}(r) = {} & \frac{2I_a cos(\beta)\,\delta(r - r_a)}{\pi L\left(m^2 sin^2\beta - \left(\frac{l\pi r_a}{L}\right)^2 cos^2\beta\right)}\times \\ & [imsin\beta\,(cos(k_l(z_a + a))\,exp(-2imn\pi) - cos(k_l(z_a - a))) \\ & - k_l r_a cos\beta\,(sin(k_l(z_a + a))\,exp(-2imn\pi) - sin(k_l(z_a - a)))] \end{aligned} \tag{23}$$

where n is the number of helix turns and $\beta = atan\,(n\pi r_a/a)$ is the helical angle. Also, the amplitude of j_z for the Nagoya III antenna can be obtained from Eq. (23) as a special case of helical type when the helical turn number n is zero.

For all antennas, only odd m modes ($m = \pm1, \pm3, \pm5\ldots$) are excited in terms of Fourier transform. In addition, considering the efficiency of simulation and convergence of resistance with (l, m) mode, the number of (l, m) mode we compute is given in Tab. 2.

Antenna type	(l_n, m_n)	$Re(Z)[\Omega]$
Double saddle	$(30, 35)$	1.76
Nagoya III	$(30, 35)$	3.52
Half-turn helical	$(30, 13)$	7.40
1 turn helical	$(30, 11)$	16.53
2 turn helical	$(40, 9)$	10.44
3 turn helical	$(40, 9)$	5.30

Table 2. The number of computed (l, m) modes and the resulting plasma resistance in nominal case. The l_n and m_n mean the number of (l, m) modes, respectively. For example, $l_n = 40$ means $l = [1, 40]$ is selected, $m_n = 9$ means $m = [-9, 9]$ is selected.

B. Influence of antenna geometrical parameters

1. *Double saddle family*

Considering the similarities, Nagoya III antenna is discussed in this section as a special double saddle antenna, which an arc angle $\theta_t = \pi$. Fig. 3(a) describes the variation of resistance when the arc angle increases. It shows that a larger angle generally yields a larger resistance, so that Nagoya III antenna is the best case within the family of double saddle antennas.

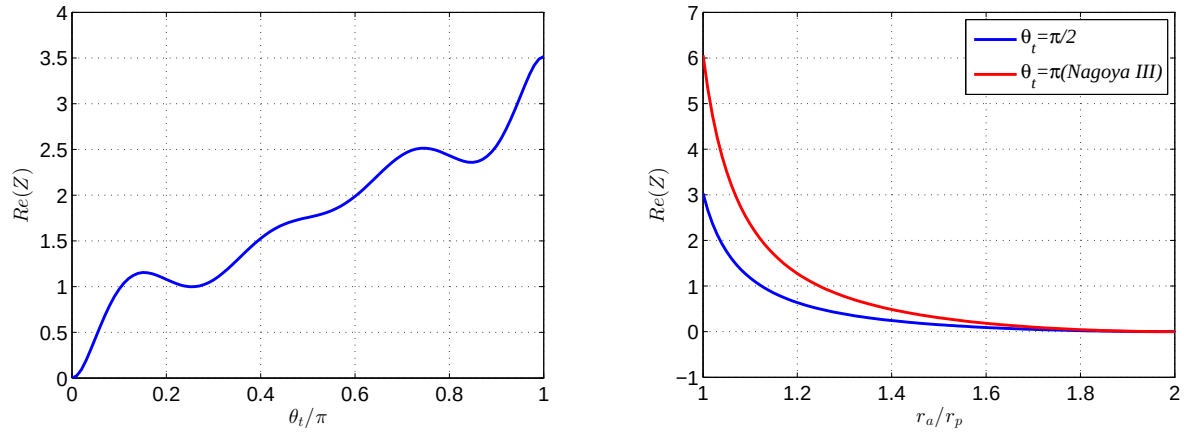

(a) Extend angle θ_t

(b) Radius of antenna r_a

Figure 3. Resistance varying with the extend angle θ_t and antenna radius r_a for double saddle antenna family.

In order to rule out the influence of θ_t on the other parameters, two cases when $\theta_t = \pi/2$ and $\theta_t = \pi$ are discussed for the main geometrical parameters (z_a, L_a and r_a). From the expression of the current density in Eq. 21, the axial component j_z is inversely proportional to the radius r_a. Therefore, with the radius of antenna increasing, the resistance should be reduced. The numerical results prove this prediction in Fig. 3(b), the resistance goes down varying with r_a for the two antennas. When the antenna is near the conducting wall ($r_a \approx 2r_p$), the resistance is almost zero. So, it is concluded that the radius of the antenna should be close to the plasma radius.

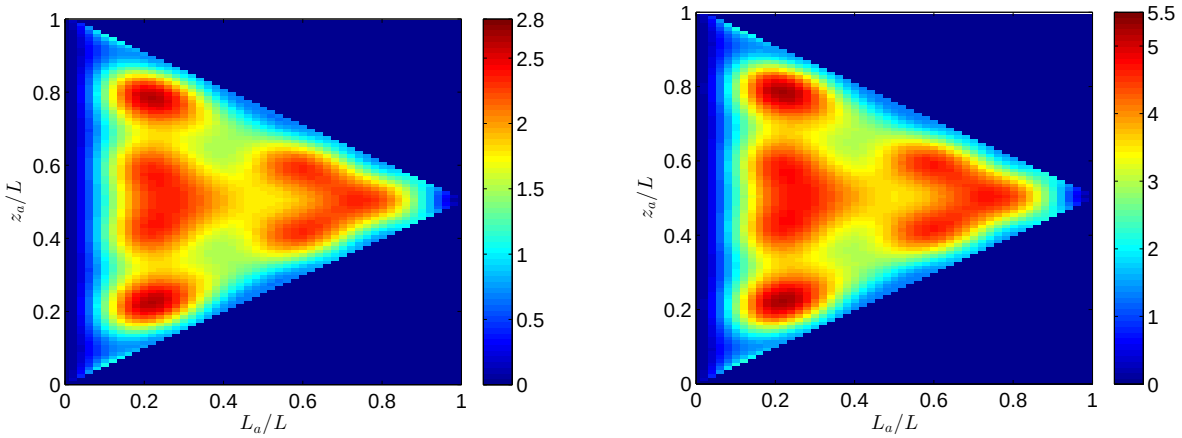

(a) $\theta_t = \pi/2$ (b) $\theta_t = \pi$

Figure 4. Resistance versus both the antenna location and the antenna length for $\theta_t = \pi/2$ and $\theta_t = \pi$.

The 2D colour maps considering both the variation of z_a and L_a are shown in Fig. 4. According to the model we use, the antenna axial length is restricted to the length of plasma column. With the variation of z_a and L_a, the current density follows the sine and cosine function. It leads to a symmetric oscillation of resistance. As we see, the maximum resistance is 5.285Ω takes place when $L_a = 0.22L$ and $z_a = 0.22L$ or $0.78L$, and amounts to 5.29Ω for the Nagoya III antenna and half that value for the case $\theta_t = \pi/2$. Very interestingly, these results show that the optimum location and length of double saddle antennas are independent of the arc angle θ_t.

2. Helical family

In this part, the analysis of geometrical parameters for helical antennas is discussed. The variation of the resistance with the relative antenna radius, for different helical antennas, is shown in Fig. 5. As before, with the double saddle antenna, plasma resistance is higher when the antenna is closer to the plasma boundary. The resistance is approximately proportional to $1/r_a$, and resistance becomes zero when $r_a = r_w$ since the conducting cage would short-circuit the antenna fields. Comparing the resistance for the different helical antennas, Fig. 5 shows that the one-turn case has the maximum resistance and no apparent rule is related to different turns. This is because the resistance of different helical antennas is strongly influence by the antenna length. Next we will show the correlations.

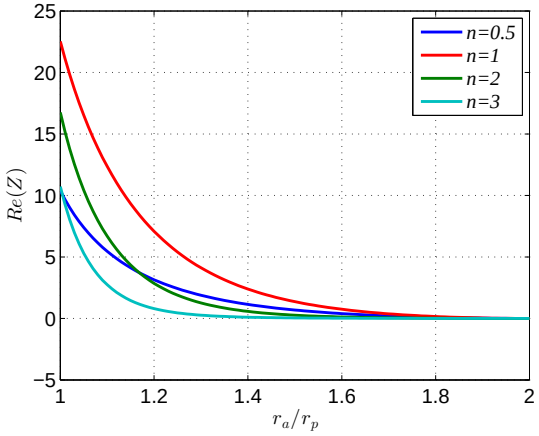

Figure 5. Resistance versus the antenna radius r_a for different number of turns.

The variations of the resistance with the antenna location and axial length for different number of turns

are described in Fig. 6. As we see, resistance values oscillate with the antenna parameters. Observing the resistance varying with the antenna axial length, the value of resistance is strongly related to L_a. With the number of turns increasing, the maximum resistance increases but requires a larger axial length of the antenna. The maximum resistance is 44.16Ω for $L_a = 0.88L$ and $z_a = 0.44L$ or $z_a = 0.56L$ in the two-turn case.

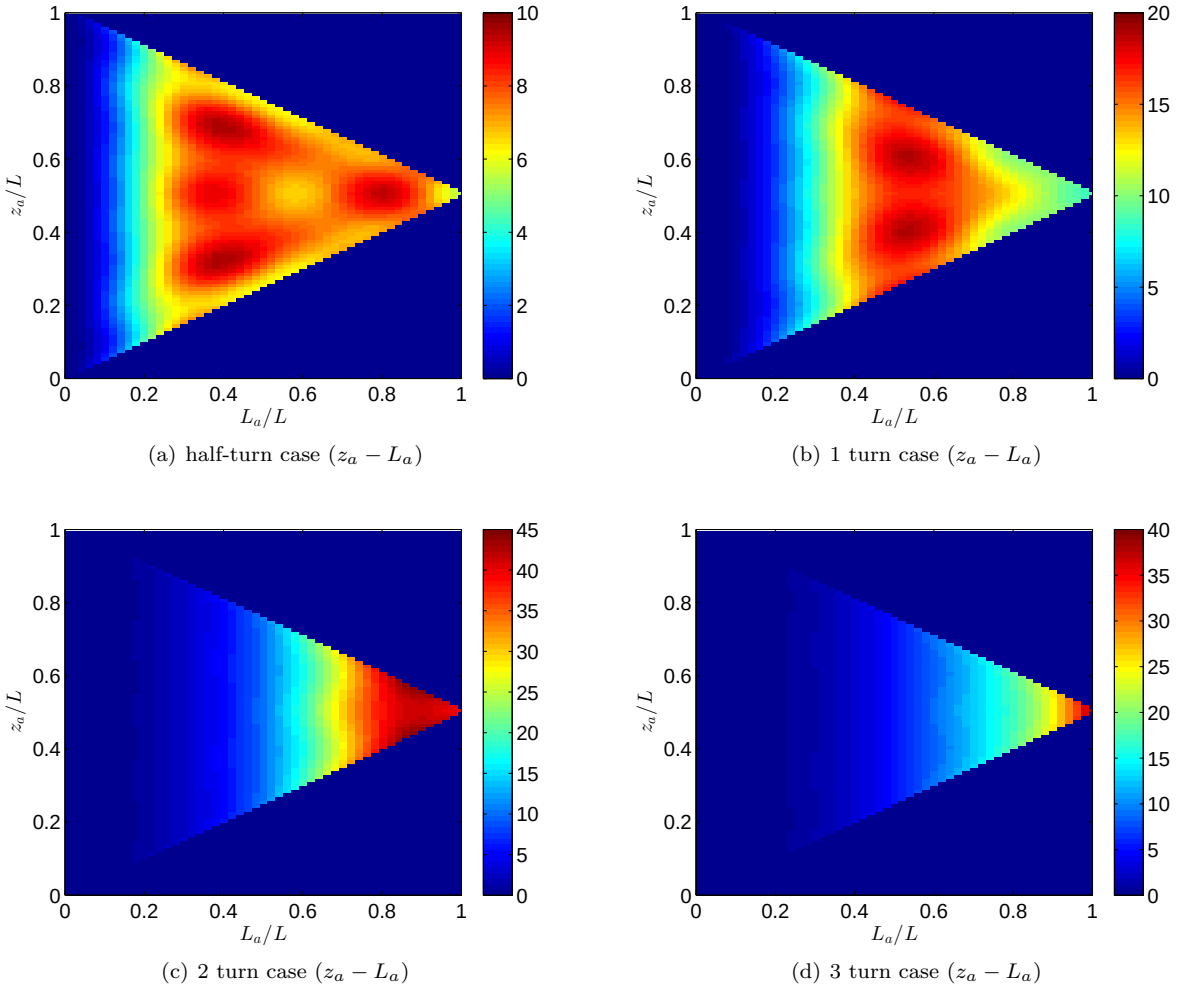

(a) half-turn case ($z_a - L_a$)

(b) 1 turn case ($z_a - L_a$)

(c) 2 turn case ($z_a - L_a$)

(d) 3 turn case ($z_a - L_a$)

Figure 6. Resistance versus both the antenna location and the antenna length for different number of turns.

In summary, it is concluded that the plasma resistance is largest when the antenna is close to the plasma column. Second, the optimum combination of antenna length L_a and antenna position z_a has been calculated for different types of antennas. For the double-saddle antenna family, the behavior is identical for the whole family, with the Nagoya III yielding the maximum resistance at some intermediate antenna axial length and locations. The helical family behaves differently. Higher turn numbers antennas can yield larger resistances but require a longer plasma column, which eventually limits the number of turns to 2 in the present case.

IV. Lower Hybrid Frequency

In this section, the anlyses of plasma-wave interaction near the lower hybrid frequency are carried out. The dispersion relation and parametric investigation are discussed in details. Furthermore, the half-turn helical antenna, which has been widely used in practices, is applied in simulations. The selected antenna parameters are the optimal combination from previous results: $L_a = 0.4L$, $z_a = L/3$ and $r_a = 1.05r_p$.

A. The dispersion relation

When the emission frequency is near the lower hybrid frequency, the influence of ions on the plasma-wave interaction cannot be neglected. The ion mass should be taken into account in the dispersion relation equations. Generally, the dispersion relation in helicon plasma can be written as a biquadratic form[15]

$$aK^4 + bK^2 + d = 0 \tag{24}$$

where: $K = kc/\omega_{pe} = kd_e$($k$ is the wavenumber, c is the light speed and d_e is the electron skin depth); a, b and d are coefficients related to the dielectric tensor components

$$\begin{aligned} a &= \hat{\kappa}_1 sin^2\theta + \hat{\kappa}_3 cos^2\theta, \\ b &= \left(\hat{\kappa}_2^2 - \hat{\kappa}_1^2\right) sin^2\theta - \hat{\kappa}_1\hat{\kappa}_3(1 + cos^2\theta), \\ d &= \left(\hat{\kappa}_1^2 - \hat{\kappa}_3^2\right), \end{aligned} \tag{25}$$

and θ is the angle between $\boldsymbol{B}_0$ and $\boldsymbol{k}$. Parallel and perpendicular wavenumbers are defined as $k_\parallel = kcos\theta$ and $k_\perp = ksin\theta$. Within the region $\omega_{pe} \gg \omega_{ce}, \omega$, neglecting ion collisionality and taking into account the relations

$$\omega_{ci} = \frac{m_e}{m_i}\omega_{ce}, \quad \omega_{pi} = \sqrt{\frac{m_e}{m_i}}\omega_{pe}, \quad \omega_{lh} = \sqrt{\frac{m_e}{m_i}}\omega_{ce}$$

the components of the dielectric tensor can be simplified to

$$\hat{\kappa}_1 = \frac{C - \alpha^2 A}{\alpha^2 - C^2}, \quad \hat{\kappa}_2 = \frac{\alpha}{C^2 - \alpha^2}, \quad \hat{\kappa}_3 = -\frac{1}{C} + A \tag{26}$$

with $A = m_e/m_i$, $C = 1 + i\nu_e/\omega$ and $\alpha = \omega_{ce}/\omega$. Solving this dispersion relation in the collisionless limit, the wave propagation regimes for argon are defined in Fig. 7. The solid straight line is the separatrix corresponding to the lower hybrid frequency. And four regimes are distinguished:

1) Inductive regime(ICR). There is no real solution for $k_\perp$. Thus, no wave propagates, rf emission penetrates only into a skin depth of the plasma column.

2) Surface wave regime(SWR). Only TG waves propagate. This is quickly damped for $\nu_e \neq 0$.

3) Double wave regime(DWR). Both helicon and TG waves propagate. The helicon wave is weakly damped and propagates the whole plasma column.

4) Low frequency helicon wave regime(LHR). Only helicon waves propagates.

The electromagnetic waves show different behaviours in the different regimes. The three regimes below the straight lines which means the emission frequency is much higher than the lower hybrid frequency has been discussed in previous paper.[12] Here, we focus on the two regimes above the line.

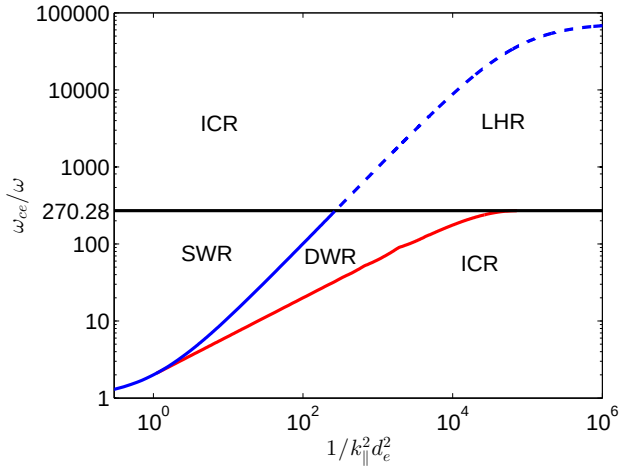

Figure 7. Wave propagation regimes.

B. Influence of frequency, magnetic field and plasma density

Fig. 8 shows the plasma resistance versus the magnetic field for different l modes and plasma densities, and the RF frequency is fixed. As we see, the resistance when $\omega < \omega_{lh}$ has numerous local peaks in the double wave regime. Then, when the lower hybrid frequency is near the wave frequency, the plasma resistance presents few sharp peaks. For $l = 2$ the resistance is up to 15.08Ω. However, for different l modes, the peak location changes with the magnetic field and the plasma density.

Fig. 9 represents the 2D colour maps of resistance varying with the magnetic field and plasma density. The different wave propagation regimes are separated by the red dashed line and the solid lines is the separatrix of the lower hybrid frequency. Below the red solid line, we can see numeral local peaks in the double wave regime. The linear relation between the magnetic field and plasma density for the plasma resistance is achieved.

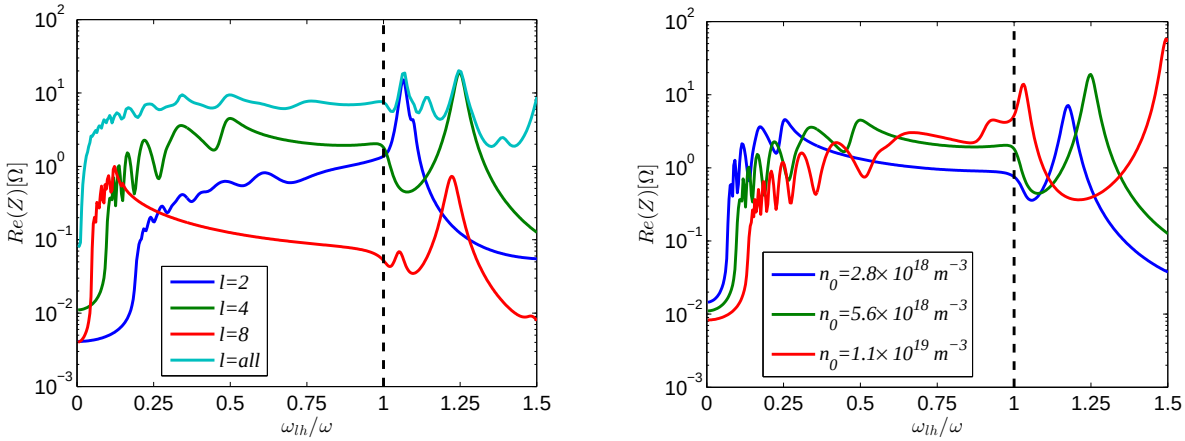

(a) l mode (b) plasma density

Figure 8. Resistance profiles varying with the ratio ω_{lh}/ω. The RF frequency is fixed and equal to 13.56MHz. The magnetic field is varied. Figure a shows the case for different l modes, the plasma density is $5.6 \times 10^{18} m^{-3}$. Figure b gives the results of different plasma density for $l = 4$.

Near the lower hybrid resonance, the peaks in the double wave regime become larger. In the regimes above this line, several isolated peaks of resistance emerge and the linear relation between the magnetic field and plasma density for the local peaks still holds. There is a transition near the lower hybrid frequency. The linear slope for the peaks is changed and the values of these peaks are much higher than the peaks in double wave regimes. It is because the change of wave propagation. Near the lower hybrid frequency, the perpendicular wavenumber of TG wave goes to infinite. The inductive mode dominates the behavior of wave propagation. Hence, the plasma becomes more inductive. In Fig. 9(d), all l modes are taken into account. More local peaks lie in the regime above the red line because of the contribution of all modes.

Fig. 10(a) gives the resistance for different RF frequency as a function of magnetic fields. All l modes are taken into account. The large peaks appear in the case of $\omega < \omega_{lh}$. The higher the applied frequency the higher the resistance is, provided that the magnetic field increases proportionally.

Fig. 10(b) which shows the resistance for different magnetic fields as a function of RF frequency proves this point. And near the lower hybrid resonance, there is a local peak of the resistance. With the frequency increasing, several modes go through the double wave regime, and lots of local peaks appear. Additionally, We can observe the proportional dependence of the resistance with the antenna frequency in terms of the Eq. (17). At a fixed ω_{lh}/ω, the power absorption is proportional to the emission frequency.

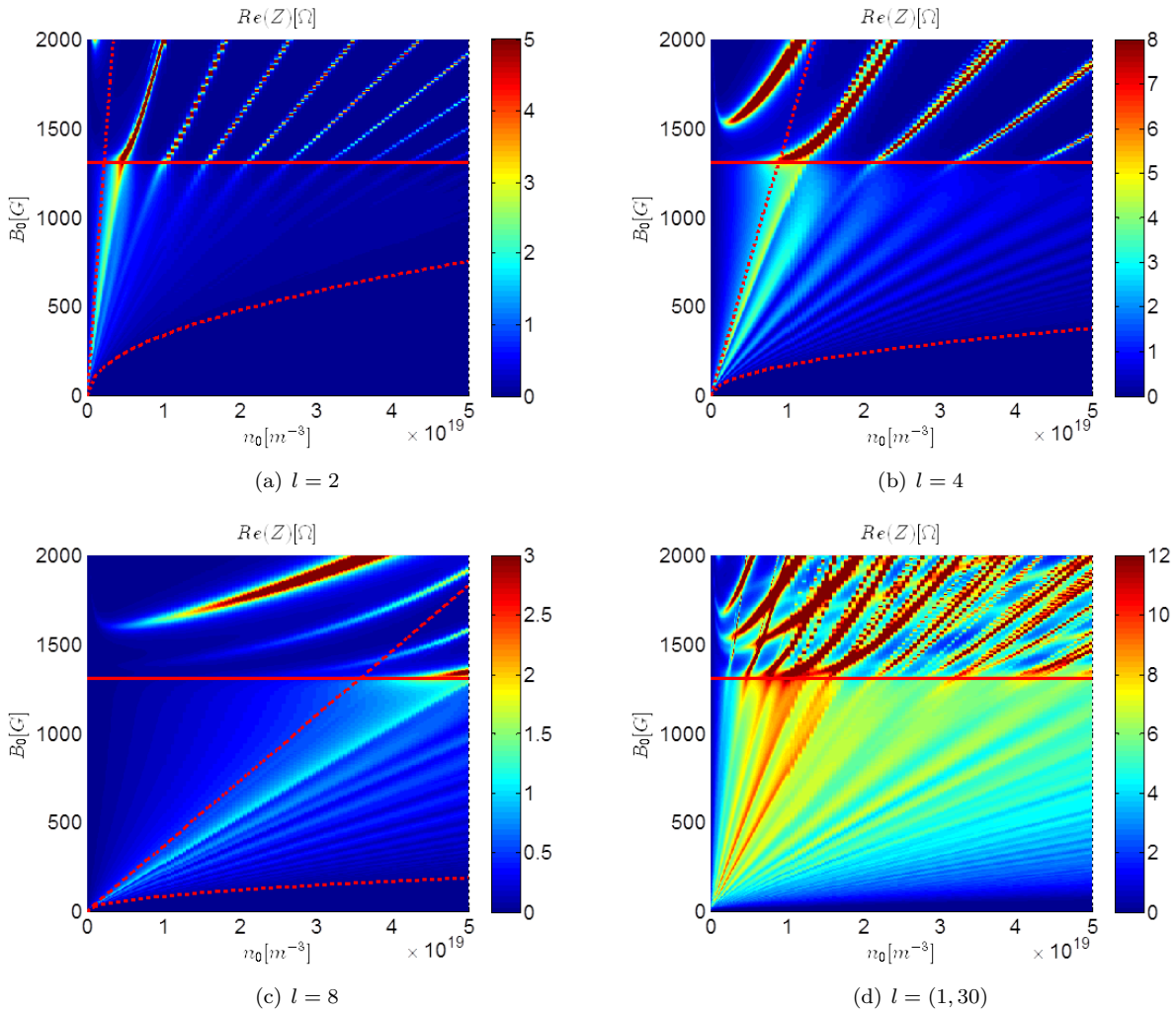

(a) $l = 2$ (b) $l = 4$

(c) $l = 8$ (d) $l = (1, 30)$

Figure 9. The 2D colour map of resistance varying with both the magnetic field and plasma density for different l mode. The red dashed line represents the different wave propagation regimes and the red solid line is the separatrix of the lower hybrid frequency.

C. Influence of electron collision frequency

The influence of electron collision frequency ν_e on the resistance is discussed in this part. Fig.11 shows the dependency of electron collision frequency and magnetic fields on the resistance for different modes. In a very low magnetic field (ICR, which means no wave propagates here), the resistance increases but still very small when the ν_e becomes larger. Because no resonance occurs in this regime, the power absorption only depends on collisions. In resonance regimes(DWR,SWR and LHR), the resistance has a local maximum for each magnetic field with changing the electron collision frequency, and then the resistance goes down if ν_e increases. When ν_e reaches up to a specific value, the resistance tends to be a constant. It illustrates that in a specific range, the collision frequency influences the resonance largely. Furthermore, a very large ν_e is not beneficial for the power deposition.

Observing the variation of different magnetic fields in the range of $\omega > \omega_{lh}$, the value of ν_e which can make the resistance get the maximum become small. It means that only a very small range of electron collsion frequency can effect the resistance in a high magnetic field. For a relatively large ν_e, the resistance becomes a constant. However, a different behavior appears when $\omega < \omega_{lh}$. In a wide range of ν_e, the resistance keeps a very high value if the magnetic field makes it reach a local peak.

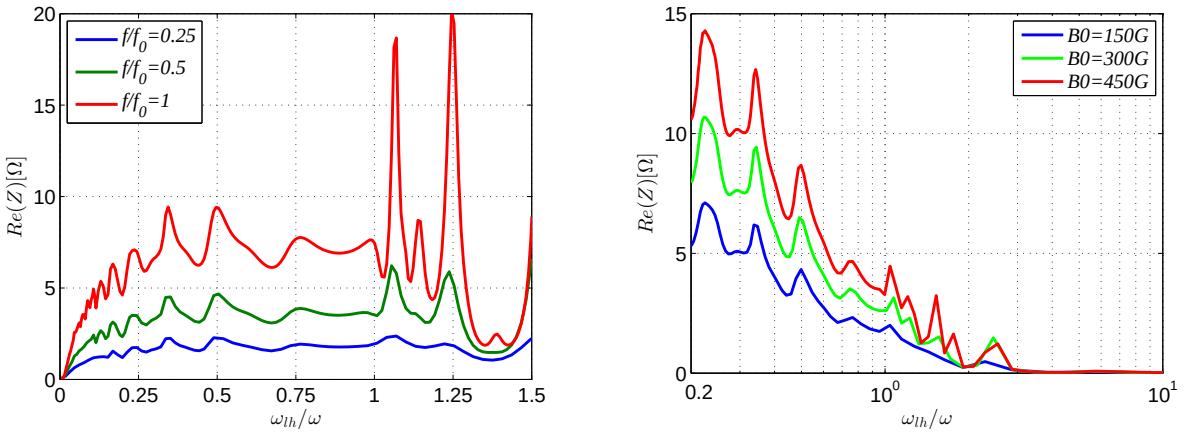

(a) $B_0 - \omega$ case (b) $\omega - B_0$ case

Figure 10. Plasma resistance versus magnetic field and wave frequency. Figure a shows the resistance as a function of magnetic field with different frequency. The nominal frequency f_0 is $13.56MHz$. Figure b shows the resistance as a function of frequency with different magnetic fields.

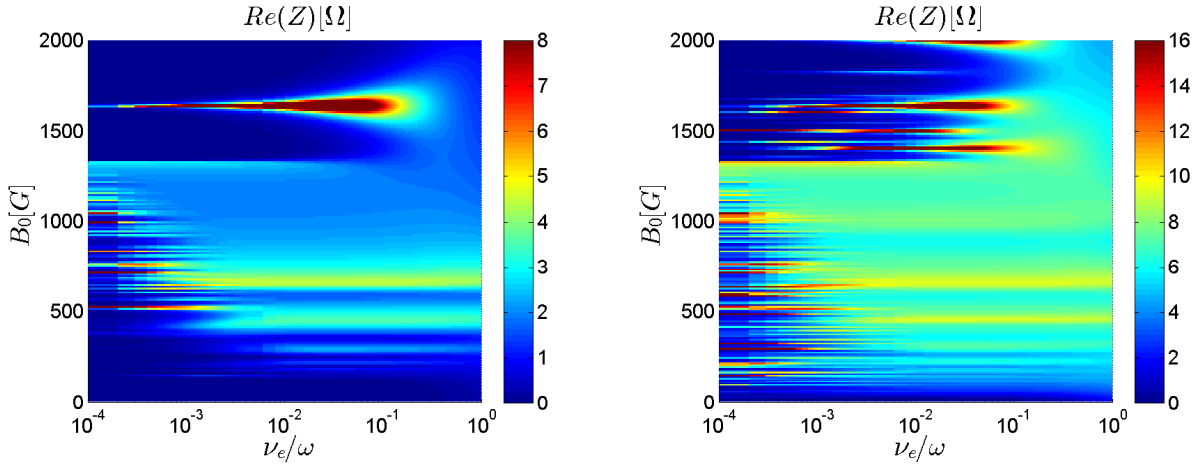

(a) $l = 4$ (b) $l = (1, 30)$

Figure 11. The 2D colour map of resistance varying with both the magnetic field and electron collision frequency for different l mode.

V. Conclusions

The parametric investigation of plasma-wave interaction has been carried out in details in order to optimize the plasma-antenna design of Helicon Antenna Thruster(HAT). Maximizing the antenna-plasma resistance is proposed to as a main optimization criterion to evaluate the overall efficiency of helicon source.

Several typical types of antennas are compared to look for the optimum antennas and geometrical parameters. With the antenna radius increasing, the resistance becomes smaller for all the types of antennas. Moreover, it goes to zero if $r_a \approx r_w$ because of the conducting wall. The Nagoya III antenna can give the maximum resistance in the double saddle antenna family since the resistance increases with the arc angle being larger. The optimum combination of antenna length L_a and antenna position z_a is calculated for different types of antennas. For the helical antenna family, with the number of turns increasing the maximum resistance raises but requires longer antenna length. Therefore, it concluded that the 2 turns helical antenna provides the maximum resistance for this thruster.

The parametric investigation near the lower hybrid frequency is illustrated. The wave propagation regime including ICR, DWR, SWR and LHR are defined according to the dispersion relation of helicon plasmas.

The different behaviors of wave propagation in these regimes are demonstrated. When the frequency is near the lower hybrid frequency, the plasma resistance can reach a local peak because of the lower hybrid resonance. The linear relation between the magnetic field and plasma density is still satisfied but a transition leads to a change of slope. The plasma resistance is proportional to the frequency and the relation between the frequency and magnetic field is linear. The influence of electron collsion frequency on the resistance depends on the wave resonance and the resistance tends to be a constant for large collsion frequencies.

Acknowledgments

This work has been supported by ESA Project(4000107292/12/NL/CO) and Spains R&D National Plan(ESP2013-41052-P). One of authors, Bin Tian, is supported by a PhD grant from the Chinese Scholarship Council. The authors thank the valuable contributions from the contract partner SENER and from ESA's officer J.A. Gonzalez del Amo.

References

[1]E. Ahedo, "Plasmas for space propulsion," *Plasma Physics and Controlled Fusion*, Vol. 53, 12, 124037, 2011.

[2]E. Ahedo and Jaume N., "Helicon thruster plasma modeling: Two-dimensional fluid-dynamics and propulsive performances," *Physics of Plasmas*, 20, 043512, 2013.

[3]S. Pottinger, V. Lappas, C. Charles and R. Boswell, "Performance characterization of a helicon double layer thruster using direct thrust measurements," *Journal of Physics D: Applied Physics*, 44, 235201, 2011

[4]M. West, C. Charles, and R. Boswell, "Testing a Helicon Double Layer Thruster Immersed in a Space-Simulation Chamber," *Journal of Propulsion and Power*, 24, 134, 2008.

[5]Chen F, "Plasma ionization by helicon waves," *Plasma Physics and Controlled Fusion*, Vol. 33, 339, 1991.

[6]K.P. Shamrai and V. B. Taranov, "Resonance wave discharge and collisional energy absorption in helicon plasma source," *Plasma Physics and Controlled Fusion*, 36, 1719-1735, 1994.

[7]Cho, S. and Lieberman, M., "Self-consistent discharge characteristics of collisional helicon plasmas," *Physics of Plasmas*, Vol. 10, 882-890, 2003.

[8]K.P. Shamrai and V. B. Taranov, "Volume and surface rf power absorption in a helicon plasma source," *Plasma Sources Sci. Technol.*, 5, 474-491, 1996.

[9]Shamrai, K. P., V. P. Pavlenko, and V. B. Taranov. "Excitation, conversion and damping of waves in a helicon plasma source driven by an m= 0 antenna," *Plasma physics and controlled fusion.*, Vol. 39, 505, 1997.

[10]Cho, S., The field and power absorption profiles in helicon plasma resonators," *Physics of Plasmas*, Vol. 3, 4268, 1996.

[11]R. Boswell, "Very Efficient Plasma Generation by Whistler Waves Near the Lower Hybrid Frequency," *Plasma Physics and Controlled Fusion*, Vol. 26, 1147, 1984.

[12]B. Tian, E. Ahedo and J. Navarro-Cavalle, "Investigation of Plasma-wave Interaction in Helicon Antenna Thrusters," *The 50th AIAA/ASME/SAE/ASEE Joint Propulsion Conference& Exhibit*, AIAA Paper No. 2014-3475, 2014.

[13]Cho, S., The role of the lower hybrid resonance in helicon plasmas," *Physics of Plasmas*, Vol. 7, 417-423, 2000.

[14]Yun, S. M., Kim, J. H., and Chang, H. Y., Frequency dependence of helicon wave plasmas near lower hybrid resonance frequency," *Journal of Vacuum Science & Technology A*, Vol. 15, 673-677, 1997.

[15]Lieberman, M. and Lichtenberg, "A. Principles of plasma discharges and materials processing," *Wiley-Blackwell*, 2005.

[16]D. Pavarin, "Design of 50W Helicon Plasma Thruste," *The 31th International Electric Propulsion Conference*, IEPC Paper No. 2009-205, 2009.

[17]T. Ziemba, J. Carscadden, J. Slough, J. Prager, and R. Winglee, "High Power Helicon Thruste," *The 41th AIAA/ASME/SAE/ASEE Joint Propulsion Conference& Exhibit*, AIAA Paper No. 2005-4119, 2005.

[18]Laeur, T., Charles, C., and Boswell, R., "Characterization of a helicon plasma source in low diverging magnetic fields," *Journal of Physics D: Applied Physics*, Vol. 44, 2011.

[19]E. Ahedo, "Plasma Dynamics in a Helicon Thruster," *EUCASS Advances in Aerospace Sciences, Progress in Propulsion Physics*, Vol. IV, 2011.

[20]Martinez-Sanchez and Pollard J, "Spacecraft electric propulsion-an overview," *Journal of Propulsion and Power*, 14, 688-99, 1998.

[21]E. Ahedo, "Two-dimensional supersonic plasma acceleration in a magnetic nozzle," *Physics of Plasmas*, 17, 073501, 2010.

[22]D. Martinez, E. Ahedo, "Plasma-wave interaction in a helicon thruster," *The 32nd International Electric Propulsion Conference*, IEPC-047, 2011.

[23]Kamenski, I. V., and G. G. Borg. "An evaluation of different antenna designs for helicon wave excitation in a cylindrical plasma source," *Physics of Plasmas*, Vol. 3, 4396-4409, 1996.

[24]J. Navarro-Cavalle, M. Merino, E. Ahedo, M. Ruiz and V. Snchez. "Design of Helicon Plasma Thruster subsystems," *The 50th AIAA/ASME/SAE/ASEE Joint Propulsion Conference& Exhibit*, AIAA Paper No. 2014-3699, 2014.